Published in final edited form as:
Prostate. 2013 December ; 73(16): 1761–1775. doi:10.1002/pros.22713.

Maturation of the developing human fetal prostate in a rodent xenograft model

Camelia M. Saffarini[1], **Elizabeth V. McDonnell**[1], **Ali Amin**[1,2], **Daniel J. Spade**[1], **Susan M. Huse**[1], **Stefan Kostadinov**[1,3], **Susan J. Hall**[1], and **Kim Boekelheide**[1]

[1]Department of Pathology and Laboratory Medicine, Brown University, Providence, Rhode Island, USA 02912.

[2]Department of Pathology and Laboratory Medicine, Rhode Island Hospital, Providence, Rhode Island, USA 02903

[3]Department of Pathology and Laboratory Medicine, Women and Infants Hospital, Providence, Rhode Island, USA 02903

Abstract

Background—Prostate cancer is the most commonly diagnosed non-skin cancer in men. The etiology of prostate cancer is unknown, although both animal and epidemiologic data suggest that early life exposures to various toxicants, may impact DNA methylation status during development, playing an important role.

Methods—We have developed a xenograft model to characterize the growth and differentiation of human fetal prostate implants (gestational age 12-24 weeks) that can provide new data on the potential role of early life stressors on prostate cancer. The expression of key immunohistochemical markers responsible for prostate maturation was evaluated, including p63, cytokeratin 18, α-smooth muscle actin, vimentin, caldesmon, Ki-67, prostate specific antigen, estrogen receptor-α, and androgen receptor. Xenografts were separated into epithelial and stromal compartments using laser capture microdissection (LCM), and the DNA methylation status was assessed in >480,000 CpG sites throughout the genome.

Results—Xenografts demonstrated growth and maturation throughout the 200 days of post-implantation evaluation. DNA methylation profiles of laser capture micro-dissected tissue demonstrated tissue-specific markers clustered by their location in either the epithelium or stroma of human prostate tissue. Differential methylated promoter region CpG-associated gene analysis revealed significantly more stromal than epithelial DNA methylation in the 30 and 90-day xenografts. Functional classification analysis identified CpG-related gene clusters in methylated epithelial and stromal human xenografts.

Corresponding author: Kim Boekelheide, Department of Pathology and Laboratory Medicine, Brown University, Box G-E5, Providence, Rhode Island, 02912. Tel: (401)-863-1783, Fax: (401)-863-9008, kim_boekelheide@brown.edu..

Competing Interests: K. Boekelheide is an occasional expert consultant for chemical and pharmaceutical companies, including Akros, Pfizer, Zafgen, and Bristol Myers Squibb. K. Boekelheide owns stock in, and is a consultant for, CytoSolv, an early stage biotechnology company developing a wound healing therapeutic based on growth factors. These activities are unrelated to the current work but are mentioned in the spirit of full disclosure.

Conclusion—This study of human fetal prostate tissue establishes a xenograft model that demonstrates dynamic growth and maturation, allowing for future mechanistic studies of the developmental origins of later life proliferative prostate disease.

Keywords

Human fetal prostate; immunohistochemistry; xenotransplantation; DNA methylation

Introduction

Prostate cancer is the most commonly diagnosed non-skin cancer in men, with approximately 240,000 new cases per year, and is the second leading cause of male cancer-related deaths in the United States (1,2). Serum prostate-specific antigen (PSA) test has aided in screening for potential cases of prostate cancer (3). However the etiology and early development of prostate cancer remain obscure despite vast knowledge about its symptoms and progression. Development of relevant fetal prostate tissue models can contribute mechanistic insight into potential early life origins of prostate carcinogenesis.

Not surprisingly, many researcher look to older cohorts in search of the origins of prostate cancer. However, autopsies have shown that prostate cancer-related lesions begin early in adulthood, between 20 and 30 years of age, indicating that prostate cancer begins long before it is clinically apparent (4). Persistent prostatic abnormalities have been observed following early life exposures to diethylstilbestrol (DES), an estrogenic endocrine disrupting chemical, in human fetal prostate tissue grown in athymic nude mice (5,6) suggesting that early life exposures may play an important role. In addition, elevated maternal endogenous estrogen levels during gestation can induce squamous metaplasia from the 24th week of gestation that can persist until 1-4 weeks after birth in the human prostate (7). These extra layers of basal cells degenerate and the epithelium returns to a typical phenotype once estrogen levels return to normal after birth (8-10). This phenotypic transformation in prostate epithelium may play a role in the changes that occur within the developing prostate, thus providing evidence that the process of prostate carcinogenesis may begin as early as fetal life.

Until recently, prostate-related research has been largely restricted to rodent and two-dimensional *in vitro* models. However, limitations of *in vitro* approaches and important differences in development and morphology between the rodent and human prostate have been recognized. Differences between the rodent and human prostate underscore the importance of using a human-specific model for studying prostate carcinogenesis. Rodent prostate development is multifaceted and relies heavily on its hormonal environment. Unlike humans, rodent prostatic growth is not quiescent after birth but is constantly growing from fetal life until adulthood (11). The rodent prostate is also more structurally complex than the human, with four lobes (ventral, lateral, dorsal, and anterior) that are surrounded by loose connective tissue (12). The adult human prostate, conversely, is separated into three main zones with fibro-muscular stroma and nerve bundles throughout. Each zone is affected by different disease processes. The central zone (25% of prostate mass) demonstrates the greatest resistance to inflammation and prostate cancer, while the peripheral zone (70% of

prostate mass) is prone to inflammation and most carcinomas. The smaller transitional zone predominates in the periurethral region (about 5% of prostate mass) and is the site of benign prostatic hyperplasia (13). These differences between rodent and human pathology present challenges in comparing a specific lobe of the rodent to a specific zone of the human (14). Importantly, unlike humans, rodents do not idiopathically develop prostate cancer; this presents an additional challenge in assessing lesions seen in animal models (15). These pronounced species differences have the potential to confound prostate-related research based traditionally on rodent models, raising the question of comparability between human and rodent prostate research. Variability of the histopathology and disease states of prostate cancer adds additional complications to the study of prostate carcinogenesis (14), underscoring the value of working directly with human tissue.

To confirm the success of the present human to rodent xenograft model, it was important to determine whether the human fetal prostate tissue was capable of differentiation into an adult phenotype. Maturation was assessed beginning at the earliest stages of development, when communication occurs between the epithelial and mesenchymal components (11). Cross-talk between these prostatic cell types is essential for proper development; in humans, this begins as early as the 11^{th} and 12^{th} weeks of gestation in the urogenital sinus mesenchyme (16,17). Androgens promote the growth and canalization of solid epithelial buds to form single ducts that then give rise to a complex ductal network. The mesenchyme is particularly important, as it is androgen responsive and expresses paracrine-acting proteins that promote proliferation of the epithelium (18). Paracrine interactions between mesenchymal and epithelial cell types induce proliferation and differentiation of the stromal and smooth muscle phenotype (19). In humans, the prostate continues to develop until birth and then enters a phase of quiescence that lasts until a surge of androgens during puberty triggers increased prostatic growth into early adulthood. At this point, no significant further growth is seen until symptoms of benign prostatic hyperplasia (BPH) develop in older men (11).

The present study explores the extent, to which xenografted human fetal prostate tissue can recapitulate normal prostate growth and development, with the additional aim of evaluating developmental DNA methylation pattern changes in the individual prostatic compartments. While xenotransplantation has been used for a number of years, this detailed molecular and phenotypic characterization of the growth of human fetal prostate tissue over an extended period of time is novel. The current study demonstrates growth and development of xenografted human prostate at both early and late life stages using a variety of immunohistochemical markers to evaluate maturation of both epithelial and stromal compartments. Analysis of early and later-life effects is strengthened by the inclusion of data on compartment-specific DNA methylated genes isolated user laser-capture microdissection (LCM) from both epithelial and stromal tissues. The present study shows that human fetal prostate tissue is capable of growing and maturing normally in a rodent xenograft system. The combined use of human tissue in a rodent model, allowing the investigation of endpoints such as DNA methylation of targeted tissue types (using LCM) makes the presented human prostate xenograft model a powerful tool for elucidating early potential mechanisms of prostate cancer.

Materials and Methods

Chemicals

Corn oil (CAS#: 8001-30-7) was obtained from Sigma Aldrich (St. Louis, MO).

Animals

Adult male Crl: NIH-*Foxn1*^{rnu} Nude rats (strain code 316) that are T-cell deficient were obtained from Charles River Laboratories (Wilmington, MA). Rats were housed in cages with access to Purina Rodent Chow 5001 (Farmer's Exchange, Framingham, MA) and water *ad libitum*. Animals were kept in a continuous 12-hour alternating light-dark cycle with controlled temperature and humidity in accordance with National Institutes of Health regulations. All experimental animal protocols were reviewed and approved by Brown University Institutional Animal Care and Use Committee. All animals were acclimated to the animal care facilities environment for one week prior to surgery.

Acquisition of Human Prostate Tissue

Human tissue was obtained in compliance with the Institutional Review Board protocols. Human fetal prostate from gestational weeks 12-24 were obtained from spontaneous pregnancy losses from Women and Infants Hospital (Providence, RI). This gestational age represents a critical period of organogenesis for the prostate (16). The protocol regarding the collection of the human fetal tissue is described in De Paepe *et al*. (20). Briefly, full informed written consent was obtained post-delivery, followed by a pathologist's determination regarding the condition of the tissue. Due to certain medical circumstances, some fetuses were excluded. The medical condition and time of latency between the autopsy and xenotransplantation was recorded for each sample.

Retroperitoneal Xeno-transplant Surgery

Human fetal prostate tissues were transported to the Xenotransplantation Core Facility at Brown University as previously described (20). Tissue was kept in ice-cold Leibovitz L-15 media supplemented with gentamycin (50 μg/mL), penicillin (100 U/mL), and streptomycin (100 μg/mL). Prior to surgery, the prostate was bisected along the midsagittal plane while preserving the structure of the prostatic zones. While it is not possible to delineate the fetal prostatic zones, tissue was marked to identify the anterior-posterior axis. Tissue was further separated into equal pieces identifying its location relative to the urethra. Each prostate piece may contain a combination of the transitional, central and peripheral zones.

Renal subcapsular retroperitoneal transplantation is a well-documented and proven method for examining development in a variety of different tissues (21-23). The surgical procedure used for the present study was reported by Wang *et al*., and is briefly described here. Immunodeficient rat hosts were placed under anesthesia and a 2-cm incision was made. Fascia and muscle were spread using scissors to expose the kidney. A small nick was made in the kidney capsule and prostate tissue was placed under the capsule. Subsequently, the abdominal cavity was closed by suturing the muscle layer and closing the skin with surgical staples (22).

This model of human fetal prostate maturation in rat hosts is being developed, in part, to investigate the effects of early life hormonal exposures on later prostate morphology and function. The rats were given a subcutaneous injection of corn oil vehicle according to their body weight to use as controls to compare for hormone-treated hosts. Rats were housed without further treatment for 7 to 200 days post-implantation.

Xenograft Collection and Histological Processing

Prostate xenografts were harvested at 7 (n=1), 30 (n=2), 90 (n=2), and 200 (n=3) days post-implantation. Sample size indicates the number of human samples used in this study. These time-points were chosen to provide longitudinal perspective on prostate development within a rodent host. A caliper measurement (mm) of each prostate piece was taken prior to xenotransplantation and at the time of collection. Fold increase was calculated based upon the volume of a rectangular prism (length x width x height).

The host kidneys and implants were removed and fixed in either 10% neutral buffered formalin for paraffin or Tissue-Tek O.C.T compound (Electron Microscopy Sciences, Hatfield, PA) for frozen sections. After fixation, each xenograft was cut along the mid-sagittal line (**Figure 2, A-C**) and processed in paraffin. Samples were cut (5 μm) and stained with hematoxylin and eosin (H&E). Additional sections were used for the detection of various immunohistochemical (IHC) markers. Tissue slides were scanned into an Aperio ScanScope CS microscope (Aperio Technologies, Vista, CA) and visualized using ImageScope software (Aperio).

Immunohistochemistry

Immunohistochemical detection of prostate markers was performed in this study, using antibodies against p63 (Santa Cruz Biotechnology Inc., Santa Cruz, CA), cytokeratin (CK) 18 (Dako Cytomation, Carpinteria, CA), α-smooth muscle actin (SMA) (Sigma-Aldrich, St. Louis, MO), vimentin (Sigma-Aldrich), caldesmon (Sigma-Aldrich), Ki-67 (Dako Cytomation), prostate specific antigen (PSA) (Dako Cytomation), estrogen receptor-α (ER-α) (Dako Cytomation), and androgen receptor (AR) (Dako Cytomation). The respective concentrations used are listed in **Supplemental Table 1**. Paraffin-embedded tissue sections (5 μm) underwent antigen retrieval via 10 mM citrate buffer solution (pH 6) or Tris-EDTA buffer solution (pH 8). Avidin and biotin were blocked (SP-2001, Vector Laboratories, Burlingame, CA). The primary antibody was applied at room temperature for one hour. The appropriate secondary antibody was then used, and visualized using a horseradish peroxidase avidin-biotin complex method with peroxidase substrate 3, 3'-diaminobenzidine (Vector Laboratories) of various colors. Tissue sections were counterstained as noted with either hematoxylin or methyl green. A negative control lacking the primary antibody was run for each staining trial. Staining represents a xenograft sample size of 1, 2, and 3 for the 7, 30, and 200-day groups respectively.

Ki-67 Quantification

Tissue sections were scanned into an Aperio ScanScope CS microscope and quantified using ImageScope Software (Aperio). The scorer was blinded to sample identity and age of xenograft. The total area for each xenograft along with the total area of the ductal tissue was

calculated (mm^2). Ki-67 positive cells were counted dependent upon the identification of clear punctate nuclear staining. The total amount of positive cells was calculated based on the number of Ki-67 positive cells divided by the total area of the epithelium or stroma.

Laser Capture Micro-dissection

Human prostate xenograft epithelial and stromal compartments were isolated using the Arcturus XT Laser Capture Microdissection system (Applied Biosystems, Grand Island, NY). Frozen O.C.T.-embedded tissue sections were cut at 7 μm, and placed onto polyethylene naphthalate (PEN) membrane glass slides (Applied Biosystems), and immediately stored at −80° C freezer until further processing. Sections were rehydrated and stained according to manufacturer's protocol (24). Epithelial tissue was captured using the infrared system, while the stromal tissue was captured using the ultra-violet laser system on Arcturus Capsure Macro LCM Caps (Applied Biosystems). DNA was extracted from LCM-isolated tissue using QIAamp DNA micro kit (Qiagen, Valencia, CA), and suspended in DNA suspension buffer (Teknova, Hollister, CA).

DNA Methylation Array

Human prostate epithelial and stromal genomic DNA was sent to Yale's Center for Genome Analysis (Yale School of Medicine, West Haven, CT) for bisulfite conversion and processed via the Infinium HumanMethylation450 BeadChip Assay (Illumina, Inc., San Diego, CA) according to manufacturer's instructions, to determine the status of >480,000 methylation sites.

Statistical Analysis and visualization

GraphPad Prism (La Jolla, CA) was used for Ki-67 graph creation. Analysis of the HumanMethylation450 BeadChip Assay data was performed in R software environment (R Foundation for Statistical Computing, Vienna, Austria). Methylation values of the two different array probe sets were normalized using subset-quantile within-array normalization with the SWAN package (25). Methylation sites differentially methylated between the epithelial and stromal tissues were identified with the minfi package (26) ($N=28,236$; $q \leq 0.05$). Gene names and promoter region information were associated with the methylation sites using the R package IMA (27). Differentially methylated sites were filtered to 1,582 sites for which the difference in mean methylation levels between tissue types was greater than or equal to 33% and for which there was no ambiguity in which gene the methylation detection sequence was located (**Figure 7**). Average beta values of CpGs in the TSS1500 (promoter) region were summarized for 11 select prostate markers with specific expression in either the stroma or epithelium. Unsupervised hierarchical clustering of promoter methylation values for the subset was performed using Cluster 3.0 (28) and visualized in Java Treeview (29). Methylation values were mean-centered, and clustering was performed using centered correlation and single linkage (**Figure 6**). Functional gene classification analysis was performed using DAVID Gene Ontology analysis based upon categorical GO_BP, GO_MF, GO_CC terms (30,31) for the list of methylation sites differentially methylated by more than 33% between tissues (**Table 1**). A full list of the gene analysis

using DAVID is included in **supplemental table 2**, and a list of gene descriptions is included in **supplemental table 3**.

Results

Human prostate xenograft growth and vascularization

Initial histological investigation of un-implanted human fetal tissue at gestational week 15 revealed that epithelial cells are present but they are poorly differentiated, resulting in ducts without defined lumens. By 19 weeks gestation, prostate epithelium forms solid cords that canalize in a proximal to distal manner. By gestation week 22, the stroma establishes a connective tissue and smooth muscle appearance, surrounded by abundant vascularization (**Figure 1**).

Human fetal prostate xenografts were characterized for growth and development 7, 30, and 200 (28.6 weeks) days post-implantation. As illustrated in **Figure 2A**, the xenotransplanted renal subcapsular prostate mass was examined grossly for the presence of cysts, glandular proliferation, and vascularization both before (**Fig. 2B**) and after (**Fig. 2C)** being bisected. Histological evaluation and various immunohistochemical markers were used to assess the extent of prostatic maturation and proliferation.

Histological examination of 7 day xenografts revealed normal prostatic growth, from a proximal to distal manner, with the presence of both secondary and tertiary buds. Solid buds normally found in fetal tissue differentiated into a simple cuboidal secretory acinar epithelium encompassed by fibrous connective tissue (**Fig. 2D)**. Immunohistochemical staining for the human endothelial CD31 marker confirmed vascularization of stromal tissue (**Fig. 2E**), and associated acini with a proper arrangement of basal and luminal epithelial cells. Epithelial maturation continued at 30 days, and by 200 days post-implantation, gross observation of human fetal prostate tissue xenotransplanted into the renal subcapsular space of a rodent host demonstrated obvious growth of the tissue (**Fig. 2B**). By 200 days post-implant, the xenografts (n=3) had ~16-fold increase in weight compared to the initial implant. Gross examination of the whole-mount xenograft revealed widespread vascularization (**Fig. 2B**) and abundant glandular and stromal tissues (**Fig. 2C**). The implanted tissue differentiated into canalized acini and ducts from solid prostatic buds typical of fetal-stage tissue, indicating that the xenograft was developing rapidly within the renal subcapsular space.

Human prostate xenograft maturation

After confirming the growth and vascularization of the implants, prostate maturation was assessed using well-defined markers of the human epithelial and stromal prostate compartments (**Figure 3**). Hematoxylin and Eosin images demonstrate the vast growth of the prostate (**Fig. 3A-C**). Representative immunohistochemical epithelial markers for basal (p63), luminal (CK18), and secretory (PSA) epithelium were used. While p63 expression (**Fig. 3D-F)** remained consistent over time, CK18 increased steadily from implantation to day 200 (**Fig. 3G-I**). The implants demonstrated morphological and developmental similarities to the adult prostate at 200 days, and it was expected that the xenograft would

also demonstrate normal adult functional activity such as prostate secretions. Xenografts were stained for prostate specific antigen (PSA); as expected, PSA expression increased gradually over time with the strongest luminal staining at 200 days (**Fig. 3J-L**).

Communication between the epithelial and stromal compartments is imperative for proper prostate growth. To quantify this, two representative stromal markers, SMA and vimentin, were examined. Both markers were present and stable over time and were found in the stromal regions around the ductal tissue (**Fig. 3M-R**), which is characteristic of normal stromal maturation in smooth muscle and the mesenchymal cytoskeleton. An additional adult stromal marker, caldesmon, was used to determine whether tissue was transforming into an adult phenotype. As expected, this marker exhibited no staining at the 7 day time-point but increased over time with the most intense staining evident at day 200 (**Fig. 3SU**).

The fetal prostate undergoes significant growth during the course of normal development, therefore cellular proliferation was examined. Quantification of Ki-67 in the individual compartments over time re-enforced these qualitative impressions with the greatest amount of Ki-67 staining observed at 7 and 30 days followed by a decline in the rate of proliferation. Proliferative activity was present, but minimal, in the epithelium by 200 days post-implantation (**Figure 4A**). Immunohistochemical staining with Ki-67 demonstrated that most proliferation occurred at 7 and 30 days post-implantation in both the epithelial and stromal compartments (**Fig. 4B-C**). The 200-day implant demonstrated scattered and less frequent Ki-67 staining in the epithelium and stroma (**Fig. 4D**).

In addition to producing secretions, the human prostate responds to many hormones, including testosterone and estrogen. Two representative hormone receptors, estrogen receptor alpha (ER-α) and androgen receptor (AR) were evaluated (**Figure 5**). ER-α was present predominantly in the epithelium, but this was not exclusive, with intermittent staining seen in the stromal tissue. Staining for ER-α was weakly present on day 7, and then gradually increased in expression over time. While staining was present in both the epithelium and stroma, it was more prominent in the epithelial compartment (**Fig. 5AC**). AR staining was abundant at 7, 30 and 200 days in both the epithelial and stromal compartments (**Fig. 5D-F**).

Xenograft DNA Methylation

DNA methylation was assessed following laser capture microdissection (LCM) separation of epithelial and stromal compartments from prostate xenografts. Unsupervised hierarchical clustering analysis of genome-wide DNA methylation at more than 480,000 CpGs in 30 and 90-day human prostate epithelium and stromal samples clustered by cell type (data not shown). Additionally, analyses of DNA methylation (n=5) in the promoter regions of a set of 11-well characterized markers of epithelial and stromal tissue were predictive of tissue type in the same manner as the global analysis (**Figure 6**). These selected markers included the stromal markers vinculin (VCL), vimentin (VIM), myosin (MYH11), α-smooth muscle actin (ACTA2), caldesmon (CALD1), and desmin (DES), while epithelial markers include p63 (TP63), e-cadherin (CDH1), cytokeratins 18 and 5 (KRT18, and KRT5), and chromogranin A (CHGA). Markers were less methylated in the compartment in which they are normally expressed and more methylated in the compartment in which they are normally

repressed, corresponding with the hypothesis that low promoter methylation allows for higher gene expression levels.

Compartment-specific differential methylation of 1582 promoter region CpG locations showed greater CpG methylation in stroma compared to epithelium (**Figure 7**). CpG examination of the genes associated with these compartment-specific differentially methylated promoter region CpGs (30,31) identified gene clusters in both epithelial (12 genes identified) and stromal (74 genes identified) compartments. The results for gene clusters, number of genes (% of clustered genes), gene symbols, and enrichment scores are summarized in **Table 1**. Enrichment scores determine the importance of the genes found within each functional group (30). The majority of genes associated with increased methylated within the epithelial compartment clustered in 2 groups with enrichment scores ranging from 0.14-0.15: metal and cation binding (*IRAK3, RNF216, ZC3H2D*) and membrane-associated (*PTPLAD1, TSPAN32, APOLD1, MLXIP, MSN*) clusters. Genes associated with increased promoter CpG methylation clustered into 28 groups (**supplemental table 2**). The stromal methylated genes clustered into 5 main groups with enrichment scores ranging from 1.57-2.03. The stromal gene clusters with the greatest enrichment scores included functional groups describing cell migration and motility (*NCK2, PPARD, TNF, ITGA6, ITGB2, CEACAM1*), regulation of DNA binding (*SP100, TNF, PEX14, SMARCA4*), regulation of immune system (*NCK2, IL2RG, ITPKB, CD5)*, positive regulation of transcription (TBL1XR1, ELF1, SP100, TNF, SP1, IRF1, CITED4, SMARCA4), and negative regulation of transcription (TBL1XR1, PPARD, SP100, TNF, PEX14, LRRFIP1, SMARCA4). The stromal gene cluster list also included a group for metal and cation binding with 17 genes identified and an enrichment score of 0.12 (**supplemental table 2**).

Discussion

There is a growing need for clinically relevant models of prostate development that can answer questions about the etiology, development, and progression of prostate cancer. The present study investigates the development and use of a model to characterize human fetal prostate xenograft growth that has successfully addressed many of the confounding variables present in rodent-only models of prostate cancer. Using a previously published and reliable xenotransplant method, human fetal prostate tissue was implanted into the well-vascularized renal subcapsular space of a rodent host (22,32-35). This model has been previously used to investigate prostatic abnormalities following DES exposure, thereby providing invaluable histopathological information on the effects of exposure to a well-known endocrine disrupting chemical (5,6). This type of investigation is encouraging and welcomes new exploration into various prostate disease states. Prostate cancer is a challenging disease in that it has variations in pathology, as well as, different responses to treatments among subjects (14). The benefits of using this well-known rodent xenograft model, along with human fetal prostate tissue, will allow researchers to address key questions regarding the developmental origins of prostate cancer, identifying potential early life exposures that may predispose to prostate cancer late in life.

Human fetal prostate differentiation

In this study, the human fetal prostate implants are placed into an adult male host secreting abundant testosterone; therefore, the fetal prostate is driven by an androgenic growth and differentiation signal throughout implantation. Immunohistochemical markers for basal (p63) and luminal (CK18) cells were used to follow the growth and maturation of the epithelium. Each component of the epithelium has a different role within the ductal tissue; basal cells most likely contain prostatic stem cells imperative to sustained proliferation, while luminal cells are responsible for the creation and secretion of prostatic secretory proteins (36-40). In addition to the role of p63 in maintaining prostatic maturation, it is also frequently used as a marker for prostatic injury and basal cell hyperplasia (41,42). There are important roles for both basal and luminal cells in development, providing an explanation for their presence in the early stages of gestation. Within the human prostate, basal cells are present as early as 9 weeks gestation (43), while luminal cell differentiation increases after gestational week 22 (44). The fetal prostates used in this study showed staining that is consistent with existing age-appropriate data for both p63, found along the basal layer of acinar tissue, and CK18, found in the secretory luminal cells, providing evidence to support this model of human prostate maturation.

While the epithelium is responsible for one aspect of prostate maturation, the roles of the stroma in both epithelial cell proliferation (45) and ejaculation of prostatic secretions via muscle contraction (19) are also fundamental in the differentiation process. The present study used two key mesenchymal markers, SMA and vimentin, to evaluate stromal maturation. These markers typically appear in the human as early as 17 weeks gestation (46). Stromal staining was strongly present and maintained from 7 to 200 days post-implantation, even while the tissue was growing markedly in size.

Accelerated growth of xenografts

While the size of the human prostate steadily increases from birth until the time of puberty in males, only nominal changes occur within the glandular components. In early adulthood, the prostate undergoes significant changes in acinar growth demonstrating fully developed glands (47). Hormones play a central role in the growth and maturation of the prostate (8); therefore it was critical to understand how the hormonal environment of an adult rodent host would impact the development of this androgen-sensitive tissue. The chronically high androgen levels found in the adult rat host were expected to promote more rapid maturation than found in human tissue. This prediction of accelerated growth brought up another important factor involving the use of an adult intact rodent model. If the human prostate normally undergoes a period of quiescence from after birth until before puberty (11), then what type of changes occur by skipping this critical phase and placing the fetal prostate directly into a mature rodent environment?

To explore the concept of accelerated stromal maturation in these xenografts, caldesmon was quantified in 7, 30, and 200-day implants. Caldesmon, a protein responsible for the contractility of smooth muscle in adult human tissue (48), was not present at 7 days, but was seen at 30 days with increased staining intensity as the xenograft aged. These results support

the hypothesis that these implants are undergoing accelerated growth from the fetal stages into adulthood as a result of exposure to the adult rodent host hormonal environment.

Quantification of proliferation was assessed by Ki-67 staining, a biomarker expressed in mitotic cells (49), providing additional evidence of accelerated growth. In adult men, this staining index is used as an indicator of grade-matched cancers (50) with the strongest staining in the most poorly differentiated regions of prostate cancer (51). However, in the human fetal prostate proliferation is greatest between gestational weeks 18 and 23, with a subsequent rapid decrease after mid-gestation and almost no proliferation occurring during the period of quiescence, from 1 month postnatal through 11 years of age (8). It is not surprising that the strongest proliferative response is during gestational weeks 18-23 because the prostate undergoes organogenesis during that period and is exposed to the fetal surge of testosterone (8). We found that both epithelial and stromal proliferation was greatest in the earliest period of xenograft development at day 7, presumably a result of the testosterone-dependent prostate entering a new hormonal environment, with a subsequent rapid decline in proliferation. These results, along with the caldesmon staining, support the notion that accelerated growth is occurring, conceivably triggered by an enhanced response to the rodent host hormonal environment. While this important question is still being investigated, it is clear that in humans hormonal alterations in this early developmental period impact the rate of prostatic tissue development. The model reported here provides an appropriate system to investigate the impact of such potential hormonal alterations. The ability to capture this information broadens the scope of investigation that is possible in future research.

Prostate xenografts exhibit characteristic functional properties

The primary function of the prostate is to produce secretions that contribute a significant volume to seminal fluid. These secretions are important to successful reproduction. While the xenografts demonstrated both differentiation and accelerated growth, it was necessary to determine if they could properly maintain the adult role of producing secretions. Produced in the prostatic epithelium and present in serum, PSA has been used for prostate cancer screening (52). In older men, high levels of PSA in serum may indicate the presence of cancerous lesions that disrupt prostatic glandular architecture, allowing PSA to increase in the circulation (53). PSA is first detected at 28 weeks gestation in the human is minimally present throughout the fetal and newborn stages (16,54), and is increased in older men (52).

In this study, PSA staining was minimal at day 7 post-implantation, and increased over implant time to reach steady state levels representative of an adult phenotype. PSA production in our xenografts suggests further utility of this model for prostate-related studies that benefit from the use of human tissue in a whole-system design, capable of simultaneously monitoring growth, development and maturation.

The model also proved capable of monitoring hormone response, an increasingly important area of research as available data implicates estrogens and androgens in the progression of prostate cancer (55). The prostate relies on androgens for proper growth and cellular proliferation through AR binding (56,57), and on ER-α for glandular branching and proliferation (58). In humans, AR is first detected around 12 weeks gestation (59), and ER-α

is expressed later, typically around gestational week 16 (60); both hormone receptors increase as organogenesis advances between gestational weeks 18 and 23. Xenograft staining was strong for both receptors 7 days post-implantation, and increased at the 30-day time-point to reach a robust level of staining at 200 days. These findings accurately reflect previously published data indicating the strong presence of both androgen and estrogen receptors in stromal and epithelial cells of the developing human prostate (60-62).

DNA methylation of significant prostate genes

DNA methylation is an epigenetic alteration that regulates gene transcription, leading to changes in gene expression without altering the DNA sequence. Methylation can occur in both transcribed and non-transcribed regions within DNA, as well as in clusters called CpG islands, located near the promoter regions of genes (63). Methylation of the genome undergoes dramatic changes early in embryogenesis which continues throughout development, a time when hormones and toxicants can change the fate of gene expression through parental exposure. As an example, exposure to diethylstilbestrol can alter the methylation status of estrogen-related genes, such as the receptors ER-α and ER-β, which play critical roles in development (64).

The epithelial and stromal compartments play different roles in the development of prostatic disease (65), and recent studies have identified compartment-specific changes in DNA methylation related to prostate cancer (66-69). Witte et al. isolated primary human basal epithelial cells (70) to demonstrate that transformed basal cells in particular are capable of developing into BPH in a xenotransplantation model (71), thus providing further evidence that separating the compartments of the prostate can provide invaluable information on prostate cancer initiation and development.

We used LCM to separate the epithelial and stromal cells of the prostate xenografts for evaluation of compartment-specific DNA methylation changes. Hierarchical clustering showed that epithelium and stroma segregated based on their global methylation patterns, as well as canonical epithelial and stromal markers. This suggests DNA methylation can identify the cell type specific status in the prostate, and contribute to identifying compartment-specific genes as they may relate to prostatic disease. Further analysis showed there were 1582 promoter region associated CpG locations that were significantly differentially methylated between stroma and epithelium. Stromal CpG methylation predominated, suggesting that epithelial differentiation requires activation of a large number of genes during the early stages of development, while stromal gene expression is relatively repressed. Prostate development relies upon active communication between the epithelial and stromal compartments (72), so the developmental patterns of DNA methylation within compartments may be quite informative regarding cell-type specific interactions and programming. Further exploration of the associated genes that are highly methylated at these early time-points will provide new information and possible new avenues to pursue after exposure to common toxicants.

In addition to prostate compartment-associated DNA methylation patterns, analysis using DAVID Gene Ontology identified CpG-related gene clusters in methylated epithelial and stromal human xenografts. Categories identified in genes with expected repression

associated with epithelial differential increased CpG methylation included metal ion and cation binding, and membrane-associated genes, while categories identified in genes with expected repression associated with stromal differential increased CpG methylation included cell migration and motility, regulation of DNA binding, regulation of immune system, and positive and negative regulation of transcription. Compartment specific gene clusters may identify susceptible targets in disease development if particular genes are disturbed during prostatic growth.

The identified DNA methylation patterns found in normal prostatic development support future studies using this model to evaluate hormonal exposures implicated in prostate cancer development and associated DNA methylation alterations.

Conclusions

The present paper reports the successful development of a xenotransplant model for prostate proliferation and maturation that maximizes the benefits of using a rodent host in laboratory-based research while ensuring that the data is not skewed by species-specific variations in prostatic tissue. The use of human fetal tissue maintains the clinical relevance of the data and makes it possible to monitor the whole-system development of the prostate from the fetal stages into adulthood. The description of this model, using various cell type and differentiation specific markers, demonstrated that these human fetal xenografts are capable of progressive differentiation and growth, production of secretions, and expression of estrogen and androgen receptors. DNA methylation revealed an increase in epithelial gene expression and stromal methylation in 30 and 90-day xenografts, thus providing new information into prostatic development. With confirmation that this model recapitulates the normal processes of growth and maturation of the human prostate, future research will explore various hormonal manipulations to identify the potential etiology of prostate cancer and evaluate different therapies for prevention and treatment that are stage-specific and targeted.

Supplementary Material

Refer to Web version on PubMed Central for supplementary material.

Acknowledgements

We would like to acknowledge Paula Weston and Melinda Golde for their great work in processing human fetal prostate tissue sections. Also, we would like to recognize Dr. Simon Hayward for his support and guidance regarding the pathology of the human fetal tissue.

Funding:

Supported by U.S. Environmental Protection Agency RD-83459401, National Institute of Environmental Health Sciences 5P20ES018169-02, and Training grant in Environmental Pathology T32-ES7272.

References

1. Jemal A, Siegel R, Ward E, Hao Y, Xu J, Murray T, Thun MJ. Cancer statistics, 2008. CA Cancer J Clin. 2008; 58(2):71–96. [PubMed: 18287387]

2. Siegel R, Naishadham D, Jemal A. Cancer statistics, 2012. CA Cancer J Clin. 2012; 62(1):10–29. [PubMed: 22237781]
3. Hsing AW, Tsao L, Devesa SS. International trends and patterns of prostate cancer incidence and mortality. Int J Cancer. 2000; 85(1):60–67. [PubMed: 10585584]
4. Gann PH. Risk factors for prostate cancer. Rev Urol. 2002; 4(Suppl 5):S3–S10. [PubMed: 16986064]
5. Yonemura CY, Cunha GR, Sugimura Y, Mee SL. Temporal and spatial factors in diethylstilbestrol-induced squamous metaplasia in the developing human prostate. II. Persistent changes after removal of diethylstilbestrol. Acta anatomica. 1995; 153(1):1–11. [PubMed: 8560954]
6. Sugimura Y, Cunha GR, Yonemura CU, Kawamura J. Temporal and spatial factors in diethylstilbestrol-induced squamous metaplasia of the developing human prostate. Human pathology. 1988; 19(2):133–139. [PubMed: 3343029]
7. Andrews GS. The histology of the human foetal and prepubertal prostates. J Anat. 1951; 85(1):44–54. [PubMed: 14814017]
8. Adams JY, Leav I, Lau KM, Ho SM, Pflueger SM. Expression of estrogen receptor beta in the fetal, neonatal, and prepubertal human prostate. Prostate. 2002; 52(1):69–81. [PubMed: 11992621]
9. Marcus R, Korenman SG. Estrogens and the human male. Annu Rev Med. 1976; 27:357–370. [PubMed: 779604]
10. McPherson SJ, Ellem SJ, Risbridger GP. Estrogen-regulated development and differentiation of the prostate. Differentiation. 2008; 76(6):660–670. [PubMed: 18557760]
11. Cunha GR, Alarid ET, Turner T, Donjacour AA, Boutin EL, Foster BA. Normal and abnormal development of the male urogenital tract. Role of androgens, mesenchymal-epithelial interactions, and growth factors. J Androl. 1992; 13(6):465–475. [PubMed: 1293128]
12. Harmelin A, Danon T, Kela I, Brenner O. Biopsy of the mouse prostate. Lab Anim. 2005; 39(2): 215–220. [PubMed: 15901365]
13. McNeal JE. Normal histology of the prostate. Am J Surg Pathol. 1988; 12(8):619–633. [PubMed: 2456702]
14. Coffey DS, Isaacs JT. Requirements for an idealized animal model of prostatic cancer. Prog Clin Biol Res. 1980; 37:379–391. [PubMed: 7384094]
15. Shappell SB, Thomas GV, Roberts RL, Herbert R, Ittmann MM, Rubin MA, Humphrey PA, Sundberg JP, Rozengurt N, Barrios R, Ward JM, Cardiff RD. Prostate pathology of genetically engineered mice: definitions and classification. The consensus report from the Bar Harbor meeting of the Mouse Models of Human Cancer Consortium Prostate Pathology Committee. Cancer Res. 2004; 64(6):2270–2305. [PubMed: 15026373]
16. Xia T, Blackburn WR, Gardner WA Jr. Fetal prostate growth and development. Pediatr Pathol. 1990; 10(4):527–537. [PubMed: 1695372]
17. Kellokumpu-Lehtinen P, Santti R, Pelliniemi LJ. Correlation of early cytodifferentiation of the human fetal prostate and Leydig cells. Anat Rec. 1980; 196(3):263–273. [PubMed: 7406220]
18. Cunha GR. Role of mesenchymal-epithelial interactions in normal and abnormal development of the mammary gland and prostate. Cancer. 1994; 74(3 Suppl):1030–1044. [PubMed: 8039137]
19. Hayward SW, Cunha GR, Dahiya R. Normal development and carcinogenesis of the prostate. A unifying hypothesis. Ann N Y Acad Sci. 1996; 784:50–62. [PubMed: 8651606]
20. De Paepe ME, Chu S, Heger N, Hall S, Mao Q. Resilience of the human fetal lung following stillbirth: potential relevance for pulmonary regenerative medicine. Experimental lung research. 2012; 38(1):43–54. [PubMed: 22168578]
21. Szot GL, Koudria P, Bluestone JA. Transplantation of pancreatic islets into the kidney capsule of diabetic mice. J Vis Exp. 2007; (9):404. [PubMed: 18989445]
22. Wang Y, Revelo MP, Sudilovsky D, Cao M, Chen WG, Goetz L, Xue H, Sadar M, Shappell SB, Cunha GR, Hayward SW. Development and characterization of efficient xenograft models for benign and malignant human prostate tissue. Prostate. 2005; 64(2):149–159. [PubMed: 15678503]
23. Wang Y, Xue H, Cutz JC, Bayani J, Mawji NR, Chen WG, Goetz LJ, Hayward SW, Sadar MD, Gilks CB, Gout PW, Squire JA, Cunha GR, Wang YZ. An orthotopic metastatic prostate cancer model in SCID mice via grafting of a transplantable human prostate tumor line. Lab Invest. 2005; 85(11):1392–1404. [PubMed: 16155594]

24. Espina V, Wulfkuhle JD, Calvert VS, VanMeter A, Zhou W, Coukos G, Geho DH, Petricoin EF 3rd, Liotta LA. Laser-capture microdissection. Nat Protoc. 2006; 1(2):586–603. [PubMed: 17406286]
25. Maksimovic J, Gordon L, Oshlack A. SWAN: Subset-quantile within array normalization for illumina infinium HumanMethylation450 BeadChips. Genome Biol. 2012; 13(6):R44. [PubMed: 22703947]
26. Hansen KD, Aryee M. minfi: Analyze Illumina's 450K methylation arrays. R package version 1.4.0.
27. Wang D, Yan L, Hu Q, Sucheston LE, Higgins MJ, Ambrosone CB, Johnson CS, Smiraglia DJ, Liu S. IMA: an R package for high-throughput analysis of Illumina's 450K Infinium methylation data. Bioinformatics. 2012; 28(5):729–730. [PubMed: 22253290]
28. de Hoon MJ, Imoto S, Nolan J, Miyano S. Open source clustering software. Bioinformatics. 2004; 20(9):1453–1454. [PubMed: 14871861]
29. Saldanha AJ. Java Treeview--extensible visualization of microarray data. Bioinformatics. 2004; 20(17):3246–3248. [PubMed: 15180930]
30. Huang da W, Sherman BT, Lempicki RA. Systematic and integrative analysis of large gene lists using DAVID bioinformatics resources. Nat Protoc. 2009; 4(1):44–57. [PubMed: 19131956]
31. Huang da W, Sherman BT, Lempicki RA. Bioinformatics enrichment tools: paths toward the comprehensive functional analysis of large gene lists. Nucleic Acids Res. 2009; 37(1):1–13. [PubMed: 19033363]
32. Bennett JA, Pilon VA, MacDowell RT. Evaluation of growth and histology of human tumor xenografts implanted under the renal capsule of immunocompetent and immunodeficient mice. Cancer Res. 1985; 45(10):4963–4969. [PubMed: 4027980]
33. Morton CL, Houghton PJ. Establishment of human tumor xenografts in immunodeficient mice. Nat Protoc. 2007; 2(2):247–250. [PubMed: 17406581]
34. Priolo C, Agostini M, Vena N, Ligon AH, Fiorentino M, Shin E, Farsetti A, Pontecorvi A, Sicinska E, Loda M. Establishment and genomic characterization of mouse xenografts of human primary prostate tumors. Am J Pathol. 2010; 176(4):1901–1913. [PubMed: 20167861]
35. Zhou H, Sun HB, Huang WB, Xu Z, Su JH, Zhu JG, Jia RP, Liu J. [Phenotypic differences of stroma cells in benign and malignant human prostate tissues]. Zhonghua Yi Xue Za Zhi. 2012; 92(8):516–519. [PubMed: 22490152]
36. Xin L, Ide H, Kim Y, Dubey P, Witte ON. In vivo regeneration of murine prostate from dissociated cell populations of postnatal epithelia and urogenital sinus mesenchyme. Proc Natl Acad Sci U S A. 2003; 100(Suppl 1):11896–11903. [PubMed: 12909713]
37. Kurita T, Medina RT, Mills AA, Cunha GR. Role of p63 and basal cells in the prostate. Development. 2004; 131(20):4955–4964. [PubMed: 15371309]
38. Letellier G, Perez MJ, Yacoub M, Levillain P, Cussenot O, Fromont G. Epithelial phenotypes in the developing human prostate. J Histochem Cytochem. 2007; 55(9):885–890. [PubMed: 17478449]
39. Hayward SW, Baskin LS, Haughney PC, Cunha AR, Foster BA, Dahiya R, Prins GS, Cunha GR. Epithelial development in the rat ventral prostate, anterior prostate and seminal vesicle. Acta Anat (Basel). 1996; 155(2):81–93. [PubMed: 8828706]
40. Soeffing WJ, Timms BG. Localization of androgen receptor and cell-specific cytokeratins in basal cells of rat ventral prostate. J Androl. 1995; 16(3):197–208. [PubMed: 7559152]
41. Ud Din N, Qureshi A, Mansoor S. Utility of p63 immunohistochemical stain in differentiating urothelial carcinomas from adenocarcinomas of prostate. Indian journal of pathology & microbiology. 2011; 54(1):59–62. [PubMed: 21393879]
42. Grisanzio C, Signoretti S. p63 in prostate biology and pathology. Journal of cellular biochemistry. 2008; 103(5):1354–1368. [PubMed: 17879953]
43. Shapiro E, Huang H, McFadden DE, Masch RJ, Ng E, Lepor H, Wu XR. The prostatic utricle is not a Mullerian duct remnant: immunohistochemical evidence for a distinct urogenital sinus origin. The Journal of urology. 2004; 172(4 Pt 2):1753–1756. discussion 1756. [PubMed: 15371806]

44. Trompetter M, Smedts F, van der Wijk J, Schoots C, de Jong HJ, Hopman A, de la Rosette J. Keratin profiling in the developing human prostate. A different approach to understanding epithelial lineage. Anticancer Res. 2008; 28(1A):237–243. [PubMed: 18383851]
45. Farnsworth WE. Prostate stroma: physiology. Prostate. 1999; 38(1):60–72. [PubMed: 9973111]
46. Bierhoff E, Walljasper U, Hofmann D, Vogel J, Wernert N, Pfeifer U. Morphological analogies of fetal prostate stroma and stromal nodules in BPH. Prostate. 1997; 31(4):234–240. [PubMed: 9180933]
47. Lowsley OS. The Prostate Gland in Old Age. Ann Surg. 1915; 62(6):716–737. [PubMed: 17863467]
48. Walther S, Strittmatter F, Roosen A, Heinzer F, Rutz B, Stief CG, Gratzke C, Hennenberg M. Expression and alpha1-adrenoceptor regulation of caldesmon in human prostate smooth muscle. Urology. 2012; 79(3):745, e745–712. [PubMed: 22197205]
49. Makarewicz R, Zyromska A, Andrusewicz H. Comparative analysis of biological profiles of benign prostate hyperplasia and prostate cancer as potential diagnostic, prognostic and predictive indicators. Folia Histochem Cytobiol. 2011; 49(3):452–457. [PubMed: 22038225]
50. Wang W, Bergh A, Damber JE. Morphological transition of proliferative inflammatory atrophy to high-grade intraepithelial neoplasia and cancer in human prostate. Prostate. 2009; 69(13):1378–1386. [PubMed: 19507201]
51. Tomaszewski JJ, Cummings JL, Parwani AV, Dhir R, Mason JB, Nelson JB, Bacich DJ, O'Keefe DS. Increased cancer cell proliferation in prostate cancer patients with high levels of serum folate. Prostate. 2011; 71(12):1287–1293. [PubMed: 21308713]
52. Nash AF, Melezinek I. The role of prostate specific antigen measurement in the detection and management of prostate cancer. Endocr Relat Cancer. 2000; 7(1):37–51. [PubMed: 10808195]
53. Sikaris K. Prostate cancer screening. Pathology. 2012; 44(2):99–109. [PubMed: 22198258]
54. Wernert N, Kern L, Heitz P, Bonkhoff H, Goebbels R, Seitz G, Inniger R, Remberger K, Dhom G. Morphological and immunohistochemical investigations of the utriculus prostaticus from the fetal period up to adulthood. Prostate. 1990; 17(1):19–30. [PubMed: 1696712]
55. Nicholson TM, Ricke WA. Androgens and estrogens in benign prostatic hyperplasia: past, present and future. Differentiation; research in biological diversity. 2011; 82(4-5):184–199.
56. Taneja SS, Ha S, Swenson NK, Torra IP, Rome S, Walden PD, Huang HY, Shapiro E, Garabedian MJ, Logan SK. ART-27, an androgen receptor coactivator regulated in prostate development and cancer. The Journal of biological chemistry. 2004; 279(14):13944–13952. [PubMed: 14711828]
57. Hamilton-Reeves JM, Rebello SA, Thomas W, Slaton JW, Kurzer MS. Isoflavone-rich soy protein isolate suppresses androgen receptor expression without altering estrogen receptor-beta expression or serum hormonal profiles in men at high risk of prostate cancer. The Journal of nutrition. 2007; 137(7):1769–1775. [PubMed: 17585029]
58. Chen M, Hsu I, Wolfe A, Radovick S, Huang K, Yu S, Chang C, Messing EM, Yeh S. Defects of prostate development and reproductive system in the estrogen receptor-alpha null male mice. Endocrinology. 2009; 150(1):251–259. [PubMed: 18755802]
59. Majumder PK, Kumar VL. Androgen receptor mRNA detection in the human foetal prostate. International urology and nephrology. 1997; 29(6):633–635. [PubMed: 9477359]
60. Shapiro E, Huang H, Masch RJ, McFadden DE, Wilson EL, Wu XR. Immunolocalization of estrogen receptor alpha and beta in human fetal prostate. The Journal of urology. 2005; 174(5): 2051–2053. [PubMed: 16217392]
61. Aumuller G, Holterhus PM, Konrad L, von Rahden B, Hiort O, Esquenet M, Verhoeven G. Immunohistochemistry and in situ hybridization of the androgen receptor in the developing human prostate. Anatomy and embryology. 1998; 197(3):199–208. [PubMed: 9543338]
62. Cai G, Huang H, Shapiro E, Zhou H, Yeh S, Melamed J, Greco MA, Lee P. Expression of androgen receptor associated protein 55 (ARA55) in the developing human fetal prostate. The Journal of urology. 2005; 173(6):2190–2193. [PubMed: 15879885]
63. Li LC, Okino ST, Dahiya R. DNA methylation in prostate cancer. Biochim Biophys Acta. 2004; 1704(2):87–102. [PubMed: 15363862]
64. Edwards TM, Myers JP. Environmental exposures and gene regulation in disease etiology. Environ Health Perspect. 2007; 115(9):1264–1270. [PubMed: 17805414]

65. Ricke EA, Williams K, Lee YF, Couto S, Wang Y, Hayward SW, Cunha GR, Ricke WA. Androgen hormone action in prostatic carcinogenesis: stromal androgen receptors mediate prostate cancer progression, malignant transformation and metastasis. Carcinogenesis. 2012; 33(7):1391–1398. [PubMed: 22535887]

66. Kim JW, Kim ST, Turner AR, Young T, Smith S, Liu W, Lindberg J, Egevad L, Gronberg H, Isaacs WB, Xu J. Identification of new differentially methylated genes that have potential functional consequences in prostate cancer. PLoS One. 2012; 7(10):e48455. [PubMed: 23119026]

67. Kron K, Pethe V, Briollais L, Sadikovic B, Ozcelik H, Sunderji A, Venkateswaran V, Pinthus J, Fleshner N, van der Kwast T, Bapat B. Discovery of novel hypermethylated genes in prostate cancer using genomic CpG island microarrays. PLoS One. 2009; 4(3):e4830. [PubMed: 19283074]

68. Li LC, Carroll PR, Dahiya R. Epigenetic changes in prostate cancer: implication for diagnosis and treatment. J Natl Cancer Inst. 2005; 97(2):103–115. [PubMed: 15657340]

69. Phe V, Cussenot O, Roupret M. Methylated genes as potential biomarkers in prostate cancer. BJU Int. 2010; 105(10):1364–1370. [PubMed: 20067451]

70. Goldstein AS, Drake JM, Burnes DL, Finley DS, Zhang H, Reiter RE, Huang J, Witte ON. Purification and direct transformation of epithelial progenitor cells from primary human prostate. Nat Protoc. 2011; 6(5):656–667. [PubMed: 21527922]

71. Goldstein AS, Huang J, Guo C, Garraway IP, Witte ON. Identification of a cell of origin for human prostate cancer. Science. 2010; 329(5991):568–571. [PubMed: 20671189]

72. Hayward SW, Rosen MA, Cunha GR. Stromal-epithelial interactions in the normal and neoplastic prostate. Br J Urol. 1997; 79(Suppl 2):18–26. [PubMed: 9126066]

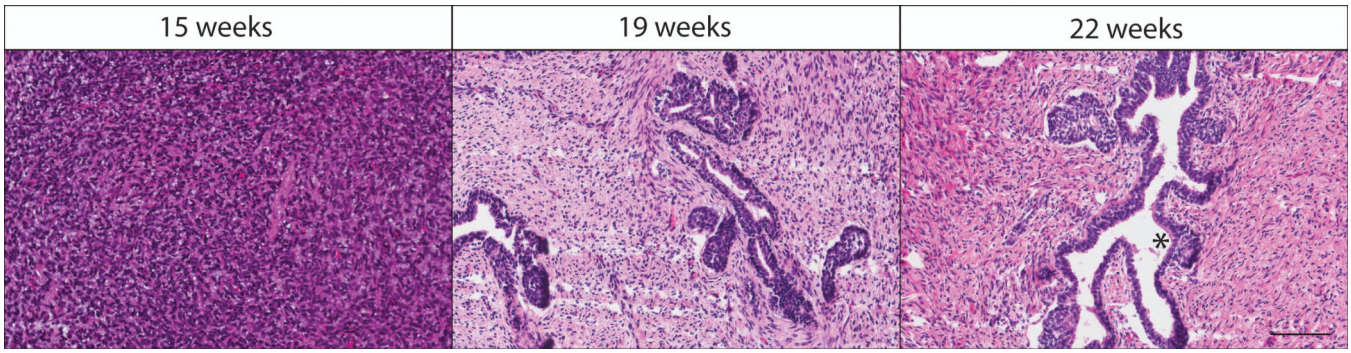

Figure 1.

Histology of un-implanted human fetal prostate tissue. Prostate tissues at 15, 19, and 22 weeks demonstrate the normal growth and progression of the stromal and epithelial compartments. Epithelial tissue originates as a mass of cells at gestational week 15, which forms solid buds encompassed by smooth muscle and connective tissue by 19 weeks gestation. These solid buds further mature and canalize in a proximal to distal manner by gestational week 22, a process that continues throughout fetal prostate development. Asterisk (*) shows a well-developed duct with lumen. Hematoxylin and Eosin staining; scale bar 100 μm.

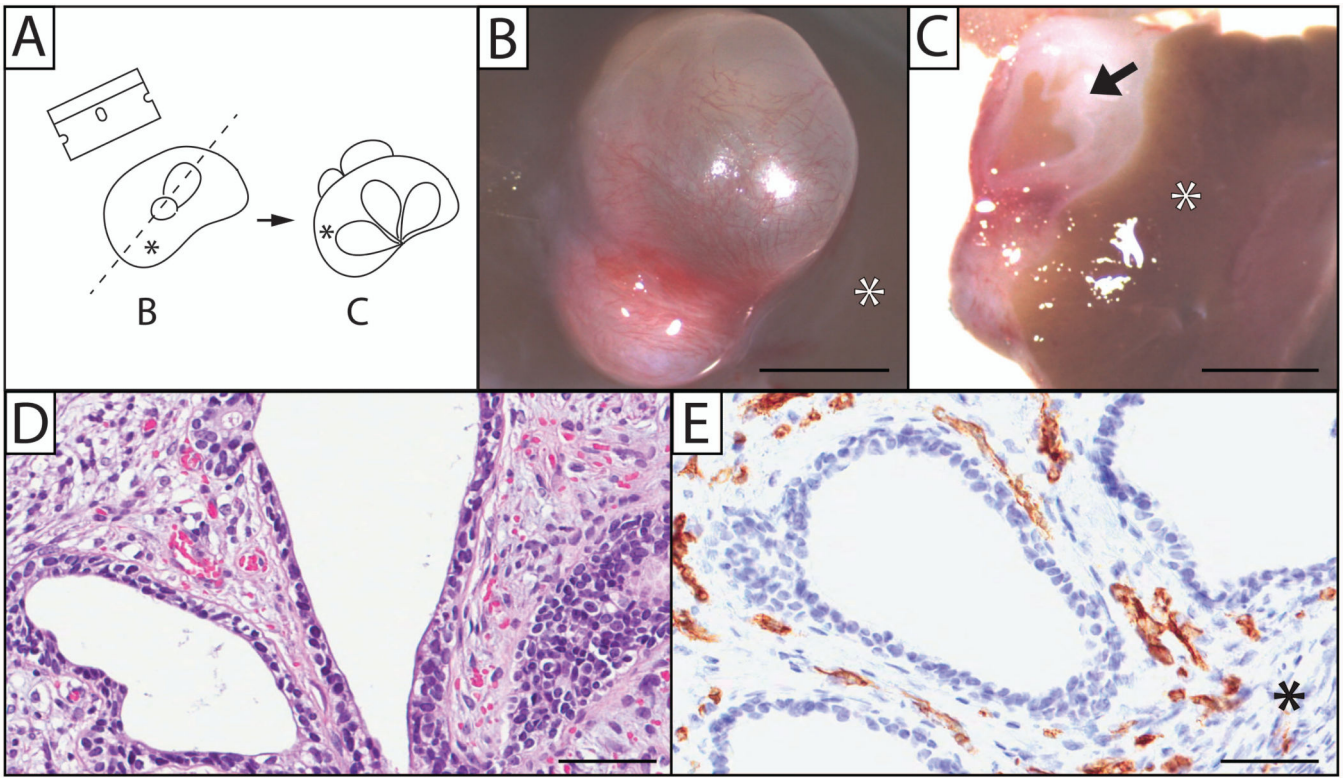

Figure 2.

Human prostate xenografts display proper growth and vascularization. (A) A drawing depicting the orientation of images shown in B and C. Human fetal prostate 200 days post-implantation into the renal subcapsular space of an immune-deficient rat host (**B**) was bisected (**C**), showing the gross appearance of ducts and stroma. Microscopically, a 7-day prostate xenograft shows normal epithelium and stromal growth (**D**), as well as vascularization that stain with the human CD31 endothelial marker (**E**). Arrow depicts ductal tissue that has canalized. Asterisk (*) indicates the location of the kidney in relation to the xenograft. Gestational age of human fetal prostate before implantation is 17 weeks (**B and C**), and 23.7 weeks (**D and E**). (Hematoxylin and Eosin staining; B, C, scale bar = 3mm; D, E, scale bar = 100 μm).

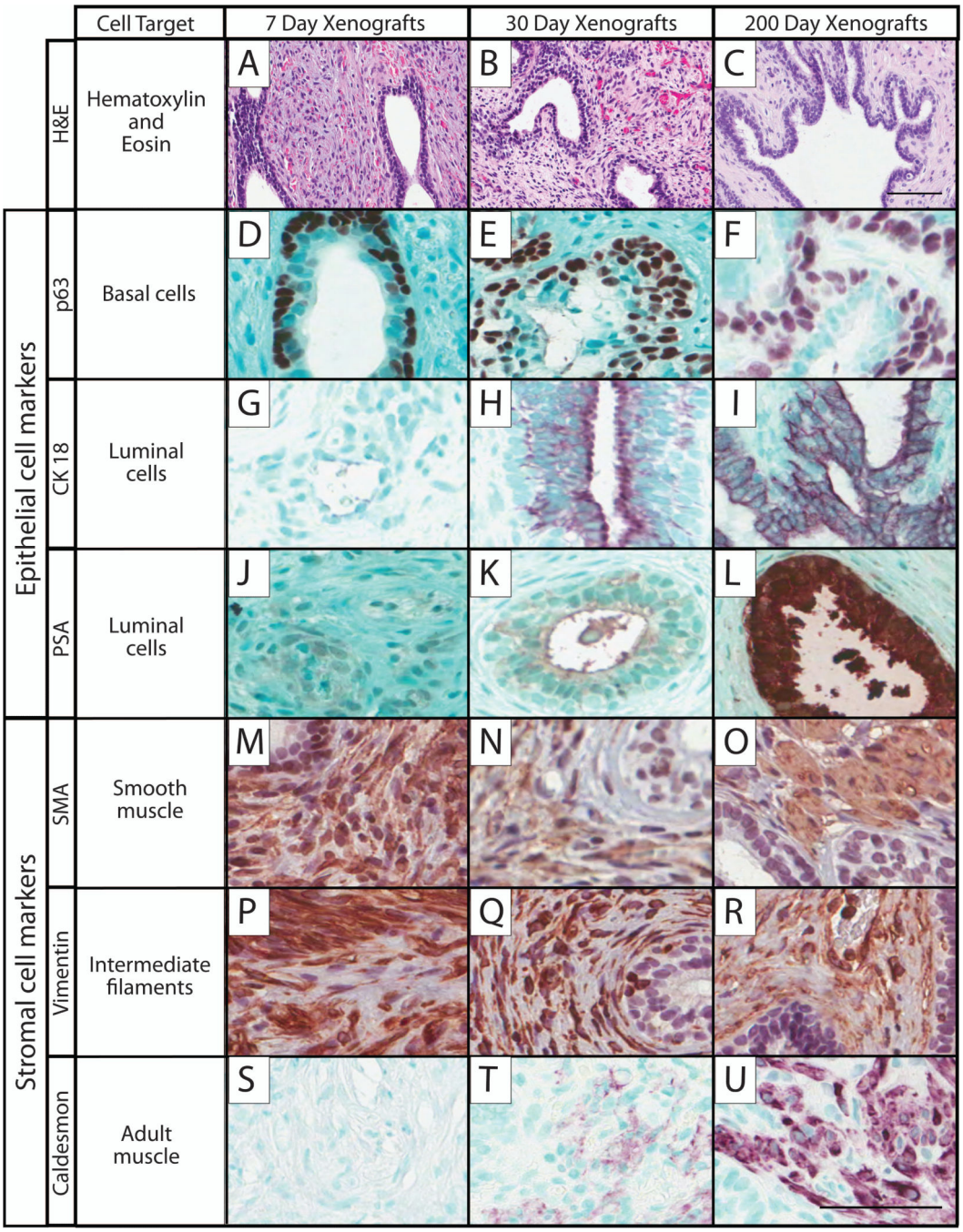

Figure 3.

Immunohistochemical staining was performed on 7, 30, and 200 day-old human prostate xenografts with markers for epithelial and stromal compartments to assess prostate growth and maturation. The different times post-transplantation are shown in the columns, and the rows are the markers, including: H&E, hematoxylin and eosin, **A-C**; p63, basal cell marker, **D-F**; cytokeratin 18 (CK-18), luminal epithelial cell marker, **G-I**; prostate specific antigen (PSA), luminal cell marker, **J-L**; α-smooth muscle actin (SMA), smooth muscle marker, **M-O**; vimentin, intermediate filaments marker, **P-R**; caldesmon, adult muscle marker, **S-U**.

Hematoxylin and methyl green counter-stain; scale bar = 50 μm; 7 day sample, 20 weeks gestation; 30 day sample, 23.7 weeks gestation; 200 day sample, 17 weeks gestation.

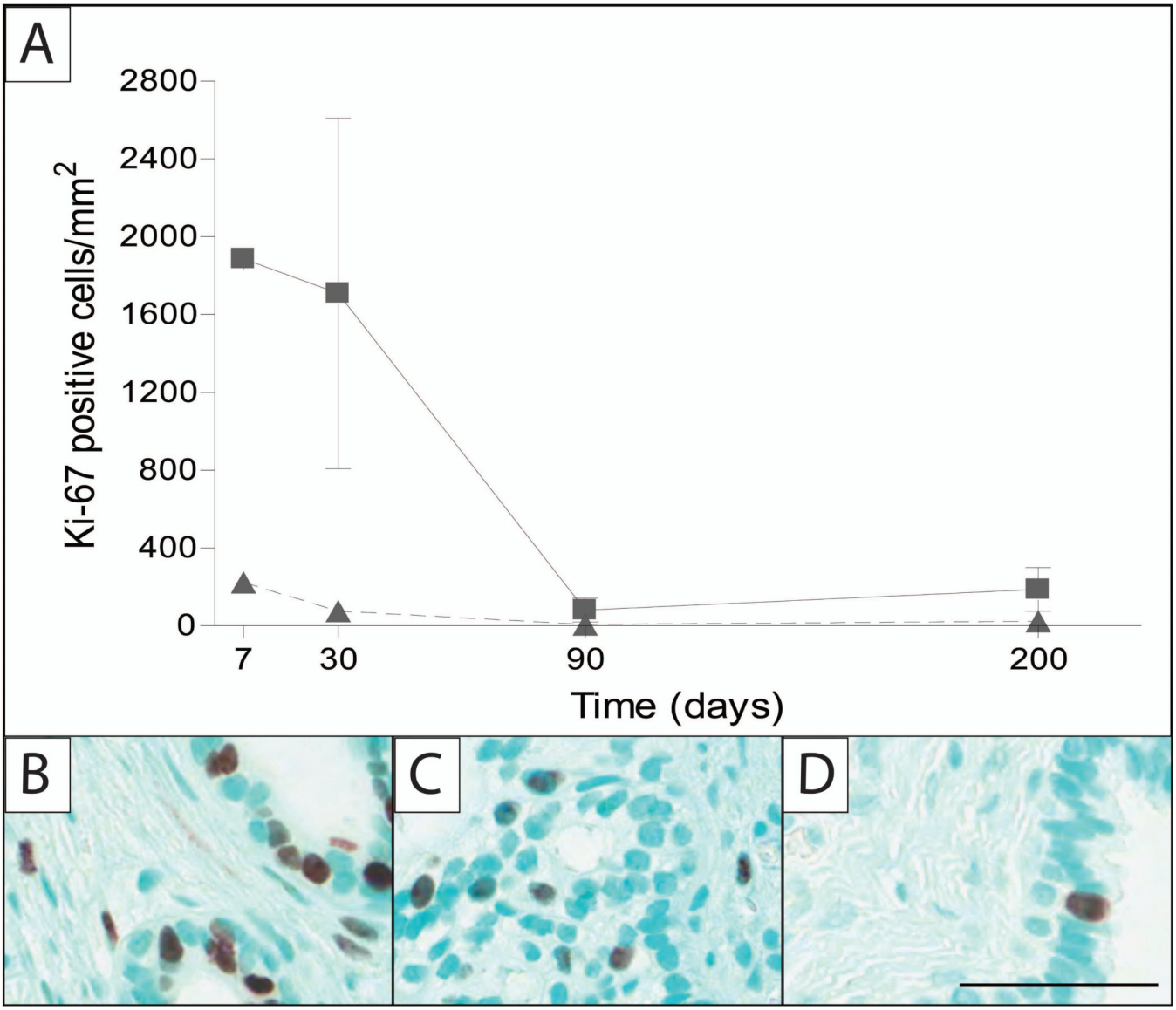

Figure 4.

Quantification of the human prostate xenografts measured at 7, 30, 90 and 200 days post-implantation. Ki-67 positive cells per area (mm^2) were quantified in the epithelial or stromal compartments at different times post-implantation (**A**). Amount of proliferation is highest at the earlier time-points (7 and 30 days), when implant growth is at its greatest. Immunohistochemical staining for ki-67, cell-proliferation marker was performed on 7 (**B**), 30 (**C**), and 200 (**D**) days post-implantation, which coincide with quantitative results. Methyl green counter-stain; scale bar = 50 μm; 7 day sample, 20 weeks gestation; 30 day sample, 23.7 weeks gestation; 200 day sample, 17 weeks gestation. Legend: ▲-epithelium; ■-stroma. Sample sizes for quantification: 7 days (n = 1), 30 days (n = 2), 90 days (n = 2), and 200 days (n =3).

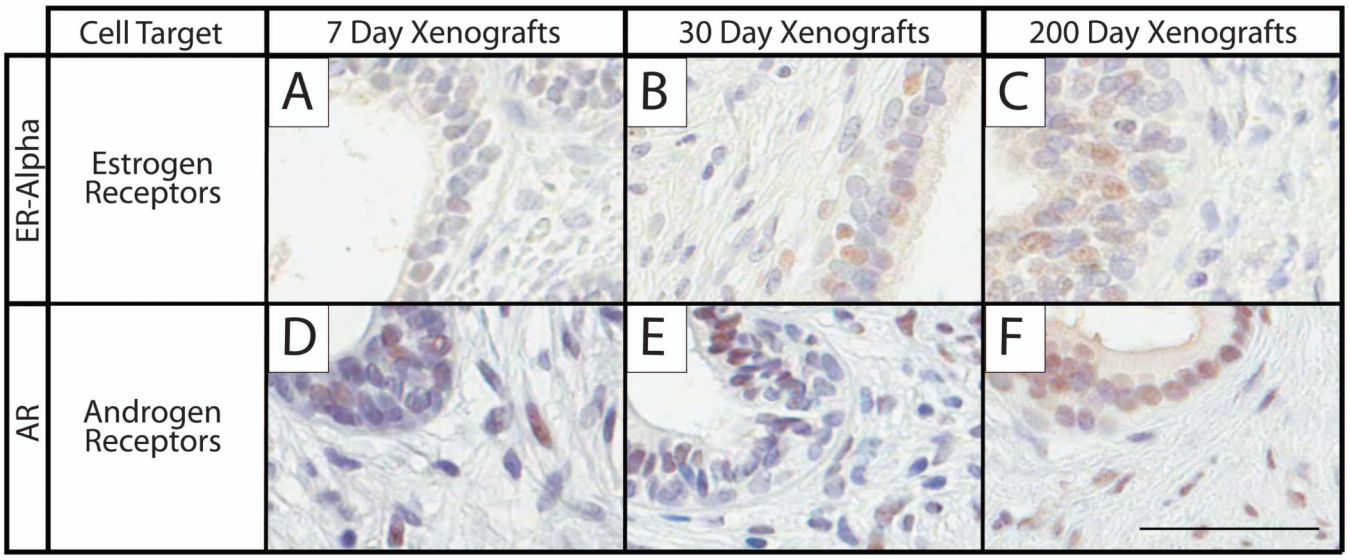

Figure 5.

Immunohistochemical staining was performed on 7, 30, and 200 day-old human prostate xenografts to assess prostate expression of essential hormone markers. The different times post-transplantation are shown in the columns, and the rows are the markers: estrogen receptor alpha (ER-alpha), estrogen receptor marker, **A-C**; androgen receptor (AR), androgen receptor marker, **D-F**. Punctate nuclear staining depicts positive cells. Hematoxylin counter-stain; scale bar = 50 μm; 7 day sample, 20 weeks gestation; 30 day sample, 23.7 weeks gestation; 200 day sample, 17 weeks gestation.

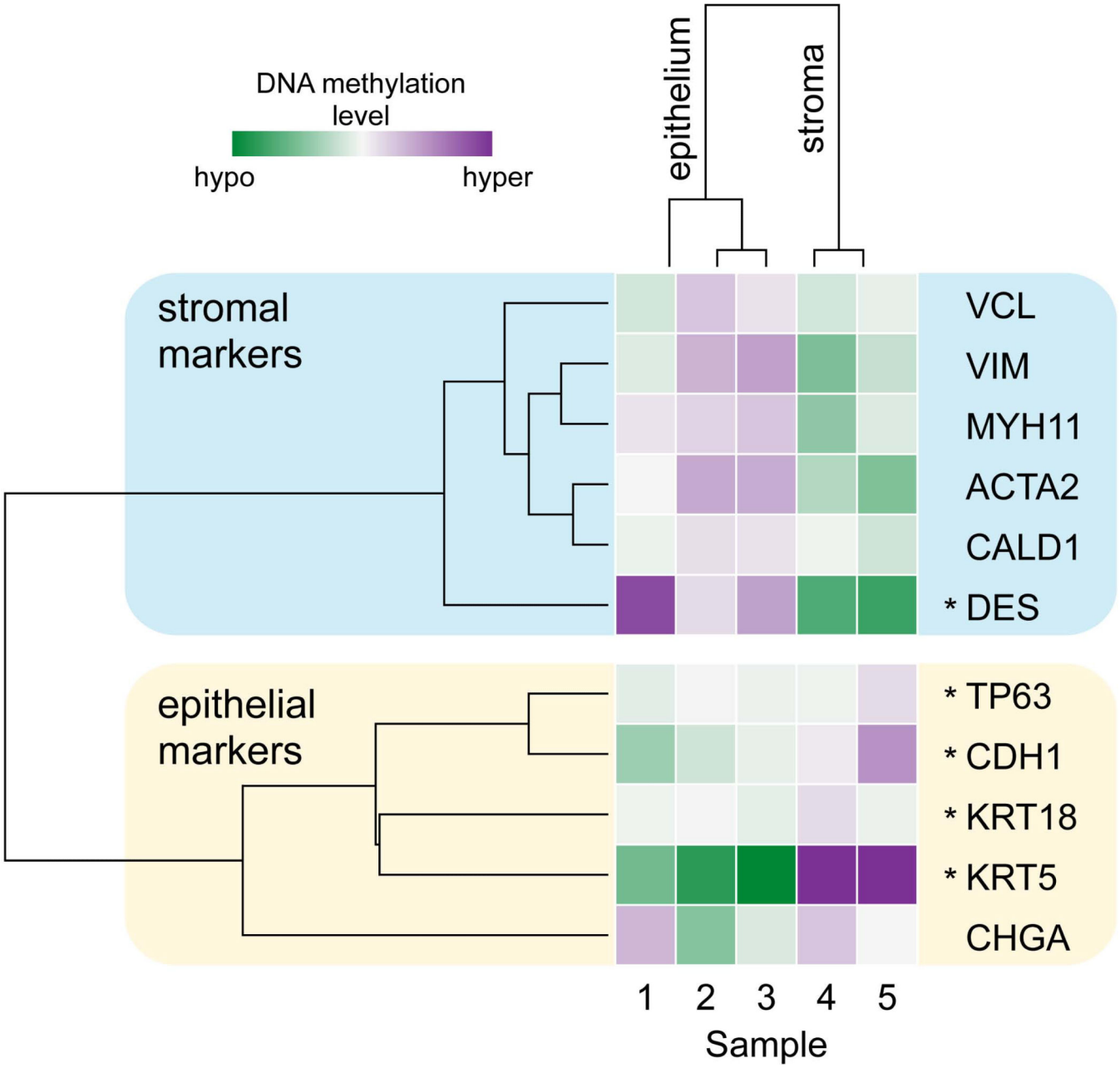

Figure 6.

DNA methylation of human prostate xenografts is different in the epithelial and stromal compartments. Heat-map of genome-wide DNA methylation analysis at promoter regions of 11 prostate marker genes specific for the epithelial (samples 1, 2, 3) and stromal (samples 4, 5) compartments. Purple color represents elevated promoter region DNA methylation, while the green color represents lowered promoter region DNA methylation relative to the mean for that promoter region. Hierarchical clustering analysis revealed that samples clustered based upon the compartment in which they are normally expressed. Sample identification is based upon age of xenograft and age of the tissue: **1**: 30 days, 20 weeks gestation; 2: 30 days, 23.7 weeks gestation; **3**: 90 days, 23.7 weeks gestation; **4**: 30 days, 23.7 weeks

gestation; **5**: 90 days, 23.7 weeks gestation. Asterisk (*), promoter regions that are significantly differentially methylated by limma with Benjamini-Hochberg correction (DES, TP63, CDH1, KRT5, and KRT18).

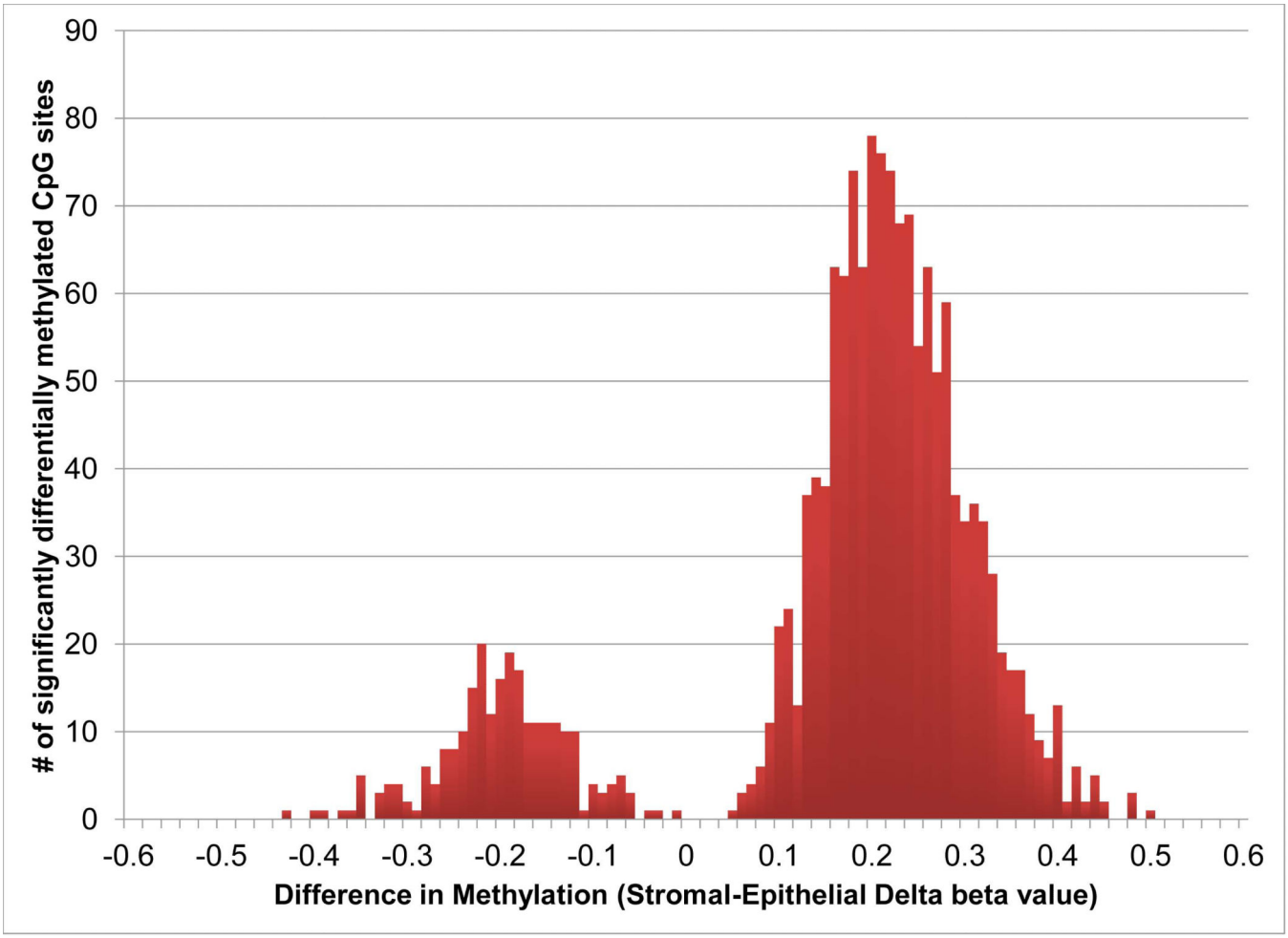

Figure 7.

Significantly differential methylation of 1582 promoter region CpG locations, in which the difference in mean methylation values between epithelial and stromal tissue was greater than or equal to 33%. Negative delta beta values indicate epithelial methylation, while positive delta beta values indicate stromal methylation. CpG methylation was greater in stromal tissue compared to epithelial tissue in 30 and 90 day xenografts.

Table 1

Functional Classification of differentially methylated CpG-associated genes in human prostate epithelial and stromal cells

Differentially methylated CpG-associated genes identified from the Illumina methylation arrays were classified into functional clusters using DAVID gene Ontology. Table summarizes the identified functional clusters, number of genes, percent of clustered genes, gene symbols, and their respective enrichment scores. Promoter region CpGs that were differentially methylated in epithelial cells clustered into two main groups with enrichment scores of 0.14-0.15. Promoter region CpGs that were differentially methylated in stromal cells clustered into 28 groups (**supplemental table 2**), with the top five represented above with enrichment scores >1.5. Gene descriptions and promoter region CpGs are located in **supplemental table 3**.

Gene functional classification	Number of genes (% of clustered genes)	Gene symbols	Enrichment scores
I. Gene clustering of epithelial cells with increased promoter region CpG methylation			
Metal ion and cation binding	3 (27%)	IRAK3, RNF216, ZC3H12D	0.15
Membrane associated (includes transmembrane region)	5 (45%)	*PTPLAD1, TSPAN32, APOLD1, MLXIP, MSN*	0.14
II. Gene clustering of stromal cells with increased promoter region CpG methylation			
Cell migration and motility	6 (8%)	*NCK2, PPARD, TNF, ITGA6, ITGB2, CEACAM1*	2.03
Regulation of DNA binding (includes transcription factor activity)	4 (5%)	*SP100, TNF, PEX14, SMARCA4*	1.78
Regulation of immune system (includes T cell, lymphocyte, and leukocyte activation)	4 (5%)	*NCK2, IL2RG, ITPKB, CD5*	1.73
Positive regulation of transcription	8 (11%)	*TBL1XR1, ELF1, SP100, TNF, SP1, IRF1, CITED4, SMARCA4*	1.71
Negative regulation of transcription	7 (9%)	*TBL1XR1, PPARD, SP100, TNF, PEX14, LRRFIP1, SMARCA4*	1.57